JOURNAL OF AGRICULTURAL AND FOOD CHEMISTRY

pubs.acs.org/JAFC Article

Ratiometric Fluorescent Metal−Organic Framework Biosensor for Ultrasensitive Detection of Acrylamide

Ziyu Gan, Wen Zhang, Muhammad Arslan, Xuetao Hu, Xinai Zhang, Zhihua Li, Jiyong Shi,* and Xiaobo Zou*

Cite This: J. Agric. Food Chem. 2022, 70, 10065−10074 Read Online

ACCESS | Metrics & More | Article Recommendations | Supporting Information

ABSTRACT: Acrylamide is a neurotoxin and carcinogen that forms during the thermal processing of food, inflicting irreversible harm to human health. Herein, a ratiometric fluorescence biosensor based on a 6-carboxyfluorescein-labeled aptamer (FAM-ssDNA) and porphyrin metal−organic framework (PCN-224) was developed. PCN-224 exhibits strong adsorption capacity for FAM-ssDNA and also quenches the fluorescence of FAM-ssDNA via fluorescence resonance energy transfer and photoinduced electron transfer. FAM-ssDNA hybridizes with complementary DNA to form double-stranded DNA (FAM-dsDNA), which is liberated from the PCN-224 surface, resulting in fluorescence recovery. However, the intrinsic fluorescence of the ligand remains unchanged. Acrylamide can create an adduct with FAM-ssDNA and inhibit the hybridization of FAM-dsDNA, thus realizing ratiometric sensing of acrylamide. The proposed biosensor displays excellent detection performance from 10 nM∼0.5 mM with a limit of detection of 1.9 nM. In conclusion, a fabricated biosensor was successfully applied to detect acrylamide in thermally processed food, and the results were consistent with those of high-performance liquid chromatography.

KEYWORDS: *ratiometric fluorescence sensing, porphyrin MOFs, DNA, thermally processed food*

INTRODUCTION

Acrylamide (AA) has been categorized as a "class 2A carcinogen" by the International Agency for Research on Cancer (IARC), owing to its neurotoxicity, genotoxicity, and carcinogenicity.[1,2] AA is produced by the Maillard reaction of asparagine and reducing sugar in food during food thermal processing over 120 °C, especially in baking and fried food, such as crisps, toasted bread, and biscuits among others.[3,4] The human body might easily absorb AA through the skin, digestive tract, and respiratory tract. Long-term exposure to AA causes genetic material damage and genetic mutations, resulting in a variety of detrimental effects on consumers' health.[5,6] The European Union (EU) specified the maximum residue levels of AA in foodstuffs including biscuits, crisps, roast coffee, and breakfast cereals to be 300−850 $\mu g \cdot kg^{-1}$.[7]

The most commonly used analytical methods for detecting AA in foods have been chromatography and mass spectrometry, both of which have a high sensitivity for AA detection.[8,9] Moreover, electrochemical analysis,[10] photoelectrochemical analysis,[11] fluorescence analysis,[12] and Raman analysis[7] methods have also been developed for AA detection. Fluorescence analysis methods present interesting advantages over these methods, including simplified operation, excellent selectivity, and high accuracy, making them suitable for a wide range of applications. Wei et al.[13] realized the AA fluorescence detection by utilizing the distance relationship between AA and carbon quantum dots with a detection range from 1 μM to 5 mM and a limit of detection (LOD) of 0.26 μM. Asnaashari et al.[14] constructed a fluorescence quenching biosensor for AA detection based on gold nanoparticles (AuNPs) and FAM-labeled double-stranded DNA (FAM-dsDNA) with a detection range from 0.1 μM to 50 mM and a LOD of 10 nM. However, most of the reported fluorescence sensors for AA detection are based on a single response signal of fluorescence enhancement or fluorescence quenching, which can be easily influenced by environmental and instrumental factors.[15] Ratiometric fluorescence sensors can reduce environmental interferences through self-calibration and realize visible detection with easy-to-differentiate color change.[16] However, ratiometric fluorescence based on metal−organic framework sensors has not been well reported. Therefore, there is still a pressing need to develop a ratiometric fluorescence sensor for AA detection.

Porphyrin metal−organic frameworks (porphyrin MOFs) also exhibit the red fluorescence of porphyrin organic ligands, in addition to notable structure properties such as large surface areas and high thermal and chemical stabilities.[17,18] Moreover, porphyrin MOFs have promising absorption of dye-labeled oligonucleotide strands through $\pi-\pi$ stacking interactions and then quench dyes' fluorescence by a photoinduced electron transfer (PET) process and fluorescence resonance energy transfer (FRET) as effective fluorescence quenchers.[19] Consequently, combining porphyrin MOFs with dye-labeled aptamers is expected to enable ratiometric fluorescence detection of AA.

Received: July 5, 2022
Accepted: July 28, 2022
Published: August 8, 2022

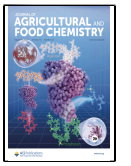

https://doi.org/10.1021/acs.jafc.2c04756
J. Agric. Food Chem. 2022, 70, 10065−10074

Scheme 1. Illustration of the Determination Process of the PCN-224 Biosensor for Rapid and Sensitive Detection of Acrylamide

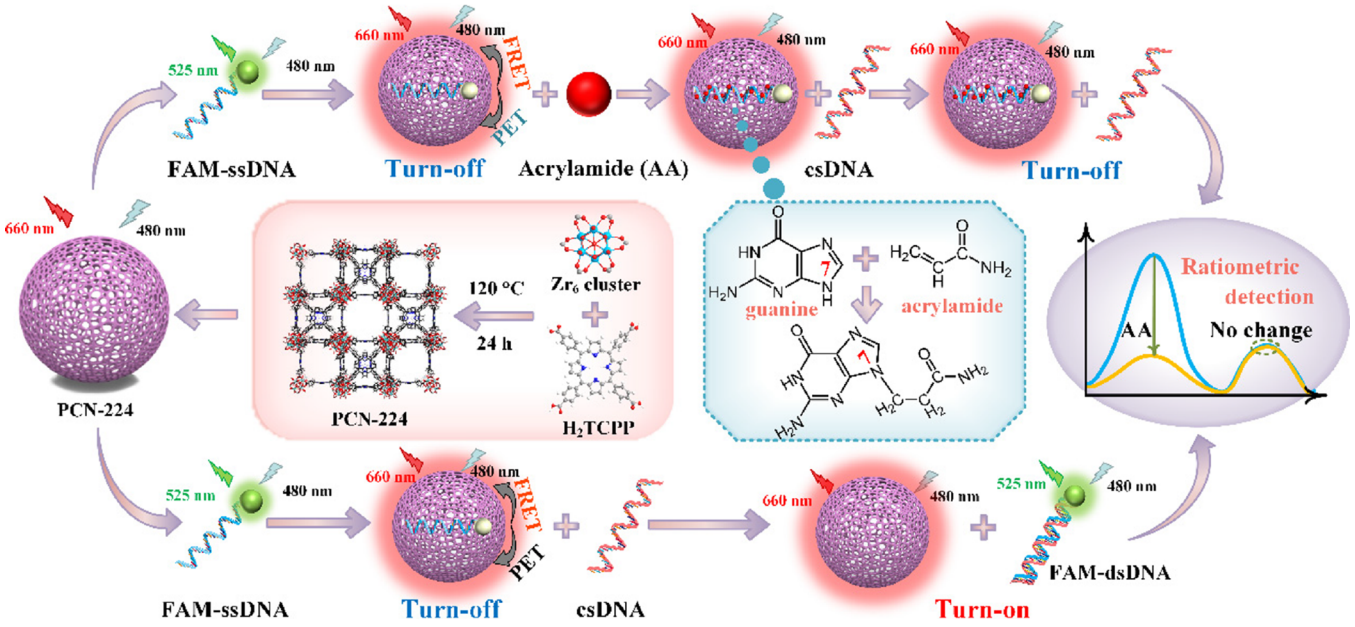

A ratiometric fluorescence biosensor has been constructed in this study for AA detection. PCN-224, a high stability zirconium-porphyrin MOF, was fabricated with red emission at 660 nm under an excitation of 480 nm. Remarkably, a 6-carboxyfluorescein (FAM)-labeled aptamer (FAM-ssDNA) was absorbed on the surface of PCN-224 and subjected to quenching fluorescence. The complementary DNA (csDNA) of FAM-ssDNA can hybridize with FAM-ssDNA and trigger conformational change, resulting in FAM-ssDNA being released from the surface of PCN-224. Fluorescence of FAM-ssDNA was restored. Conjugation of AA and FAM-ssDNA inhibited the formation of FAM-labeled double-stranded DNA (FAM-dsDNA).[14,20] We established a fluorescence biosensor for AA detection based on this approach (Scheme 1). The PCN-224 biosensor has the following advantages for sensing AA: (1) PCN-224 can strongly and effectively adsorb FAM-ssDNA through $\pi-\pi$ stacking, hydrogen bonds, electrostatic interactions, and coordination interactions; (2) fluorescence of PCN-224 (λ_{em} = 660 nm) from the organic ligand porphyrin is not affected by AA and the aptamer, thus realizing the ratiometric fluorescence detection of AA; (3) high stability and selectivity benefit complex real sample matrix detection. More importantly, the proposed PCN-224 ratiometric fluorescence biosensor is applied to real AA analyses for various natural samples of crisp and biscuit, and the obtained results are compared with high-performance liquid chromatography (HPLC) method results.

EXPERIMENTAL SECTION

Materials and Reagents. Zirconyl chloride octahydrate ($ZrOCl_2 \cdot 8H_2O$), tris (hydroxymethyl)aminomethane-hydrochloride (Tris−HCl), and AA were obtained from Aladdin Reagent Co. Ltd. (Shanghai, China). 5,10,15,20-Tetrakis (4-carboxyphenyl) porphyrin (H_2TCPP) was purchased from J&K Scientific Co. Ltd. (Shanghai, China). Benzoic acid (BA), hexane, and *N*,*N*-dimethylformamide (DMF, 99.5%) were obtained from Sinopharm Chemical Reagent Co., Ltd. QuEChERS buffer salt (containing 4 g of $MgSO_4$ and 1 g of NaCl) was obtained from High Education Research Technology Co., Ltd. (Beijing, China). AA aptamers labeled with 6-carboxyfluorescein (FAM) dye, FAM-ssDNA, 5′-FAM-ACG GCA ACA TGC CGA AGG AAC TAC CGG AAA CGG CAA ATC CTC G-3′, designed according to ref 14, and csDNA, 5′-CGA GGA TTT GCC GTT TCC GGT AGT TCC TTC GGC ATG TTG CCG T-3′ were synthesized by Sangon Biotech Co., Ltd. (Shanghai, China). Tris−HCl buffer (10 mM, pH 7.4) comprising 150 mM NaCl, 5 mM KCl, and 5 mM $MgCl_2$ was used in this study.

Apparatus. Crystal orientation was examined with an X-ray diffractometer (XRD; D8 ADVANCE, Bruker, Germany). Surface morphology was characterized by scanning electron microscopy (SEM; JSM-7800F, JEOL, Japan) and transmission electron microscopy (TEM; JEM-2100, JEOJ, Japan). SEM−energy-dispersive spectroscopy (EDS) mapping analysis was performed with a JEM-2100 equipped with a monochromatic microspot X-ray beam and EDAX (Japan). Thermogravimetric analysis was performed using an STA 448 F5 Jupiter (Netzsch, Germany) from room temperature to 800 °C with a heating rate of 10 °C min^{-1} under N_2 conditions. N_2 adsorption−desorption isotherms were examined at 77 K using a Micromeritics ASAP 2460 device (USA). PCN-224 was degassed at 150 °C for 5 h, and the surface area was calculated using the Brunauer−Emmett−Teller (BET) equation. Fourier transform infrared spectrometer (FT-IR) analysis was conducted with a Nicolet iS50 (Thermo Fisher, USA). X-ray photoelectron spectroscopy (XPS) was obtained with an ESCALAB 250 (USA). Zeta potential results were investigated using a Zetasizer Nano ZS90 analyzer (Malvern, U.K.). The fluorescence lifetimes of PCN-224 and PCN-224-FAM-ssDNA were evaluated with an FLS 1000 (Edinburgh) under an excitation wavelength of 475 nm. A UV−visible absorption spectrometer (UV-2700i, Shimadzu, Japan) and fluorescence spectrophotometer (F-98, Lengguang, China) were used to examine fluorescence behaviors. All fluorescence data were the average of three measurements.

Synthesis of PCN-224. The synthesis of PCN-224 was based on a method reported previously.[21] A Pyrex vial was used to ultrasonically dissolve $ZrOCl_2 \cdot 8H_2O$ (60 mg), H_2TCPP (20 mg), and BA (600 mg) in 12 mL of DMF. The resultant mixture was incubated in an oven at 120 °C for 24 h. Once cooled to room temperature, the purple precipitate was centrifuged (8000 rpm, 5 min) and washed thrice with DMF. Finally, the obtained solid was dried in a vacuum oven (100 °C, 12 h) for further use.

Detection of Acrylamide (AA). PCN-224 suspension (20 μL, 0.2 mg mL^{-1}) was added to 1 mL of Tris−HCl buffer containing FAM-

https://doi.org/10.1021/acs.jafc.2c04756
J. Agric. Food Chem. 2022, 70, 10065−10074

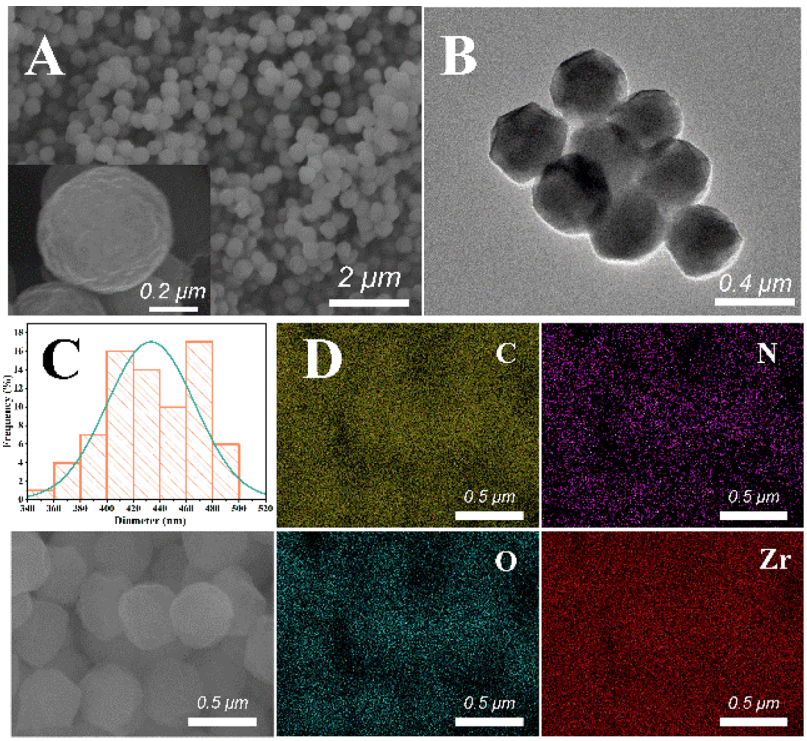

Figure 1. (A) SEM image, (B) TEM image, (C) particle size distribution, and (D) SEM mapping spectra of PCN-224.

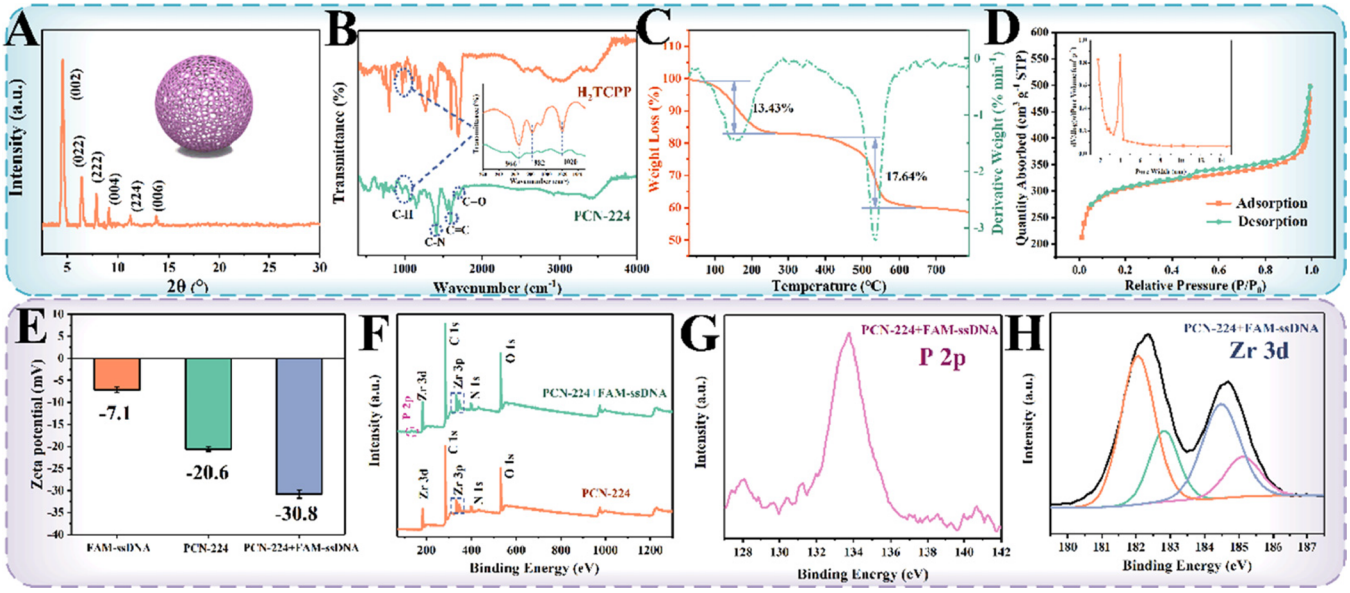

Figure 2. (A) XRD image of PCN-224. (B) FT-IR spectra of PCN-224 and H_2TCPP. (C) TGA and (D) BET spectra of PCN-224. (E) Zeta potential of PCN-224, FAM-ssDNA, and PCN-224 absorbed with FAM-ssDNA. (F) XPS spectra of PCN-224 and PCN-224 absorbed FAM-ssDNA. High-resolution XPS responses of the (G) P 2p and (H) Zr 3d core energy levels of PCN-224 adsorbed with FAM-ssDNA.

ssDNA solution (20 μL, 0.5 μM) and mixed for 12 min for AA detection. Thereafter, 50 μL of AA solutions with different concentrations was added to the above solution and incubated with the FAM-ssDNA aptamer for 60 min. Afterward, csDNA solution (20 μL, 0.5 μM) was poured and incubated for 35 min. The final AA concentration ranged from 0 nM to 8 mM. The fluorescence intensity of the above solutions was detected at λ_{ex} = 480 nm. In particular, the ratio of fluorescence found at 660 and 525 nm was considered an indicator (I_{660}/I_{525}) of AA levels. In addition, the interference studies and assays of actual samples were carried out using the same procedure. All incubation experiments were carried out in a shaker at 37 °C.

Analysis of AA in the Actual Samples. The potato chips and biscuits were obtained from a local market in Zhenjiang, China. Detection of AA in potato chips and biscuit samples was carried out according to the modified QuEChERS method.[5,22] First, the ground samples (3 g) were degreased twice with hexane (10 mL). Subsequently, 20 mL of solution mixed with deionized water and acetonitrile (v/v = 1:1) was added and ultrasonicated for 10 min. Thereafter, QuEChERS buffer salt was added and sonicated to obtain a homogeneous mixture, which was then centrifuged at 8000 rpm for 10 min. Finally, acetonitrile was evaporated by drying the supernatant under nitrogen flow at 40 °C. The treated samples were spiked with

https://doi.org/10.1021/acs.jafc.2c04756
J. Agric. Food Chem. 2022, 70, 10065−10074

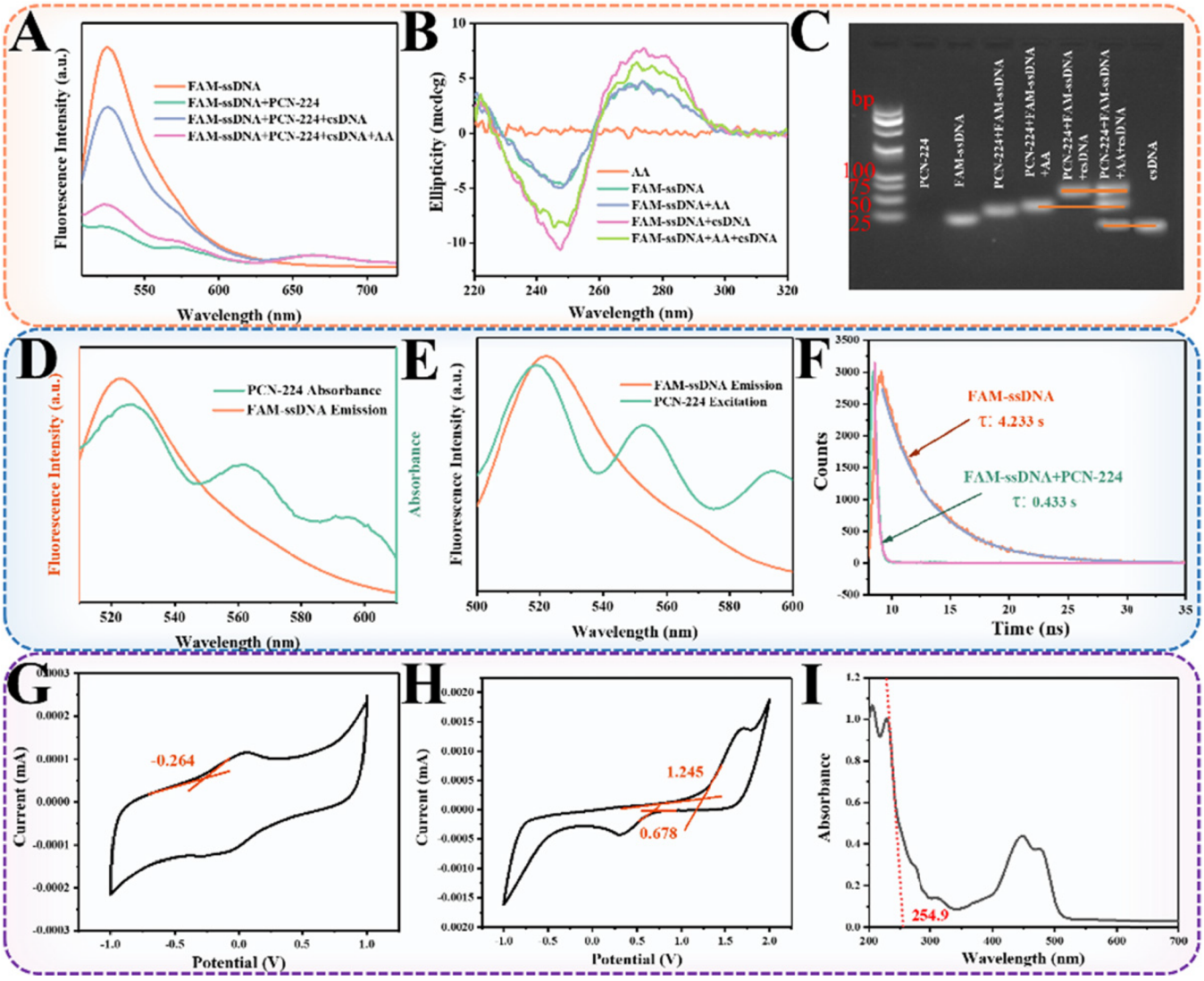

Figure 3. (A) Fluorescence spectra of FAM-ssDNA under different conditions. (B) CD spectra of FAM-ssDNA and AA under different conditions. (C) Gel electrophoresis (3% agarose). (D) Overlap between the PCN-224 absorption spectrum and FAM-ssDNA fluorescence emission spectrum. (E) Overlap between the PCN-224 fluorescence excitation spectrum and FAM-ssDNA fluorescence emission spectrum. (F) Fluorescence lifetimes of FAM-ssDNA in the presence and absence of PCN-224. The cyclic voltammograms of (G) FAM and (H) Zr−O were measured on a glassy carbon electrode in 0.1 M Bu_4NPF_6 CH_3CN solution at a scan rate of 50 mV/s. (I) Absorption spectrum of FAM.

standard AA solutions (300 and 600 $\mu g \cdot kg^{-1}$) and filtered through a 0.22 μm membrane for further analysis.

RESULTS AND DISCUSSION

Characterization of PCN-224. The morphology and size of PCN-224 were characterized using SEM and TEM. As manifested in Figure 1A, PCN-224 was a homogeneous spherical crystal with good dispersibility and an average size of 432.3 nm, which can be separated by centrifugal precipitation with simpler synthesis steps and higher yields than rod-shaped PCN-222 (Figure 1C).[19] TEM imaging of PCN-224 revealed a well-defined microstructure, proving its rough surface cubic solid sphere structure (Figure 1B). Moreover, EDS mapping analysis of PCN-224 demonstrated that PCN-224 was composed of C, N, O, and Zr elements, which was consistent with the elemental contents of the synthesized raw materials, indicating that PCN-224 was successfully synthesized (Figure 1D). The crystal structure of PCN-224 was measured using XRD patterns. As illustrated in Figure 2A, the peaks observed at 4.6°, 6.5°, 7.9°, 9.1°, 11.2°, and 13.7° were associated with the (002), (022), (222), (004), (224), and (006) crystal facets, respectively, confirming that the prepared PCN-224 exhibited identical diffraction peaks as previously reported.[21]

The surface groups of PCN-224 were further examined using FT-IR spectroscopy. As illustrated in Figure 2B, peaks at 966, 985, and 1020 cm^{-1} were assigned to the C−H oscillating vibration of the pyrrole ring.[23] The strong absorption peak at 1415 cm^{-1} was attributed to the bending vibration of C−N.[24] The C═C stretching vibration in the benzene ring was at 1600 cm^{-1}, and the band at 1738 cm^{-1} was ascribed to the C═O asymmetric stretching vibration.[25] These results demonstrated that the FT-IR peaks of PCN-224 were primarily derived from its organic ligand.

The thermal stability of PCN-224 was explored with TGA under a N_2 atmosphere. The results of TGA analysis revealed that PCN-224 had two stages of weight loss. An initial weight loss in the range of 108−208 °C was ascribed to the evaporation of DMF in PCN-224. Furthermore, the sharp

https://doi.org/10.1021/acs.jafc.2c04756
J. Agric. Food Chem. 2022, 70, 10065−10074

weight loss from 501 to 557 °C was related to the decomposition in metal−organic frameworks and organic ligands (Figure 2C). Such a long range of mass stabilization phases (210−500 °C) indicated the high thermal stability of the synthesized PCN-224.

The textural properties of PCN-224 were characterized by N_2 adsorption−desorption isotherms. As found in Figure 2D, the specific surface area of PCN-224 was determined to be 992.64 $m^2 g^{-1}$. To that end, BET thesis based on the isotherm adsorption branch in the range of $0.05 < P/P_0 < 0.30$ was used to determine the conclusion.[26] Such a large specific surface area provided the possibility for the absorption of FAM-ssDNA. Furthermore, pore size distribution of PCN-224 (Figure 2E) indicated the presence of a mesoporous structure in PCN-224, facilitating better adsorption of the aptamer. The successful synthesis of PCN-224 was confirmed by all characterization results.

Identification of the Adsorption Ability of PCN-224. PCN-224 was thoroughly characterized to study its ability to absorb FAM-ssDNA. As measured, PCN-224 had large surface areas, and its ligands (H_2TCPP) also had abundance of benzene in its conjugated π-system. As a result, the significant absorption of FAM-ssDNA on the surface of PCN-224 could be facilitated by the $\pi-\pi$ superposition between H_2TCPP and nucleobase ring structures.[27,28] EDS mapping investigation revealed the presence of P elements on the surface of PCN-224 after successful adsorption of FAM-ssDNA (Figure S1). The interaction between PCN-224 and FAM-ssDNA could be explained with zeta potential analysis. PCN-224, FAM-ssDNA, and PCN-224 absorbed FAM-ssDNA presented negative potentials of −20.6, −7.1, and −30.8 mV, respectively (Figure 2F). This outcome indicated that PCN-224 possessed weak electrostatic interaction with FAM-ssDNA.[29] Moreover, the XPS spectrum (Figure 2G) of PCN-224 with FAM-ssDNA attached showed a new peak of P2p from the FAM-ssDNA phosphate group at 133.6 eV in addition to peaks of C 1s, N 1s, O 1s, Zr 3d, and Zr 3p. The two additional new curve components at 182.8 and 185.1 eV of PCN-224 adsorbed FAM-ssDNA were obtained by decomposition due to Zr−O−P coordination (Figure 2H), as compared to the Zr 3d spectral peaks of PCN-224 at 182.4 and 184.8 eV (Figure S2).[30] Consequently, the adsorption capacity of PCN-224 originated from $\pi-\pi$ stacking, hydrogen bonding, van der Waals forces, and coordination interactions generated by the H_2TCPP ligand, Zr^{4+}, and PCN-224 structure.

Principles and Validations of the Fluorescence Assay. The detection validity of the fluorescence assay was then demonstrated by monitoring the fluorescence spectra in the presence and absence of AA in the PCN-224 biosensor. As demonstrated in Figure 3A, the fluorescence of FAM-ssDNA was quenched after being absorbed onto the surface of PCN-224. The fluorescence of FAM-ssDNA was recovered after adding complementary DNA (csDNA), which would originate from the hybridization between FAM-ssDNA and csDNA to form FAM-dsDNA. The binding affinity between FAM-ssDNA and PCN-224 was reduced by potentially masking the nucleobases and phosphate groups of FAM-ssDNA.[31] Hence, FAM-dsDNA released from the surface of PCN-224, and PET and FRET processes disappeared, resulting in FAM-ssDNA fluorescence recovery. Interestingly, AA could disrupt the fluorescence recovery process of FAM-ssDNA (Figure 3A). AA possessed high affinity for FAM-ssDNA and may form adducts with FAM-ssDNA, impeding the hybridization between FAM-ssDNA and csDNA.[32] Except for being a well-bonded hydrogen acceptor, AA was also a hydrogen bond donor for N and O atoms. As a result, AA may establish a stable hydrogen bond with the guanines of FAM-ssDNA, resulting in the formation of FAM-ssDNA-AA adducts.[20] Despite the formation of FAM-ssDNA-AA adducts, most of the nucleobases and phosphate groups in FAM-ssDNA were still exposed due to the small number of binding sites of AA and FAM-ssDNA. Therefore, the adducts failed to be released from the surface of PCN-224 and the fluorescence of FAM-ssDNA was still quenched.

To further confirm this, the circular dichroism (CD) plot of FAM-ssDNA in the presence and absence of AA was investigated. CD was an important method for studying conformational changes of the aptamer before and after binding with targets. As displayed in Figure 3B, FAM-ssDNA exhibited positive and negative peaks at 274 and 247 nm, respectively, corresponding to the base stacking effect and helical superstructure. AA possessed an extremely weak CD signal in Tris−HCl buffer. The curve of FAM-ssDNA exhibited any signal change when AA was added, revealing that the recognition between FAM-ssDNA and AA was rigid and hardly independent of conformational changes. However, FAM-ssDNA hybridized with csDNA to form a double-helical structure, resulting in significant changes in the CD signal. Furthermore, the addition of AA results in weaker CD signal change compared with the addition of csDNA only. The CD signal of FAM-ssDNA changed when AA was introduced first, followed by csDNA, which was significantly lower than the CD signal with csDNA addition only. This is because the interaction of AA with the guanine base bond was sufficient to disrupt the hydrogen bond between the guanine base and cytosine base.[33] Hence, FAM-ssDNA that failed to bind to AA can change its conformation by hybridization with csDNA, resulting in a partial alteration of CD signal.

Agarose gel electrophoresis was used to further verify the adsorption and release process of the aptamer (Figure 3C). The PCN-224 bands of adsorbed FAM-ssDNA were significantly higher than those of FAM-ssDNA itself, demonstrating the successful adsorption of FAM-ssDNA. A higher band was observed with the addition of AA, indicating the successful binding of AA to FAM-ssDNA and failure to release from the PCN-224 surface after binding. However, different bands were observed after the addition of csDNA indicating the release of FAM-dsDNA from the PCN-224 surface. The addition of AA certainly inhibited the hybridization of FAM-ssDNA with csDNA, leading to partial FAM-dsDNA formation and release.

Fluorescence Quenching Mechanism of PCN-224. Fluorescence quenching behaviors on FAM-ssDNA absorbed on PCN-224 were examined. As depicted in Figure 3C, the fluorescence excitation spectrum of PCN-224 (λ_{em} = 660 nm) overlapped well with the fluorescence emission spectrum of FAM-ssDNA at 525 nm. Furthermore, PCN-224 also exhibited a broad UV−vis absorption band that overlapped with the emission fluorescence spectrum of FAM-ssDNA (Figure 3D). It was discovered that by measuring the time-resolved fluorescence spectra of FAM-ssDNA with or without the addition of PCN-224, the fluorescence lifetime of FAM-ssDNA was reduced (Figure 3E, Table S1). The quenching mechanism was attributed to the FRET between FAM and H_2TCPP after FAM-ssDNA was adsorbed onto the surface of PCN-224, based on prior findings.

https://doi.org/10.1021/acs.jafc.2c04756
J. Agric. Food Chem. 2022, 70, 10065−10074

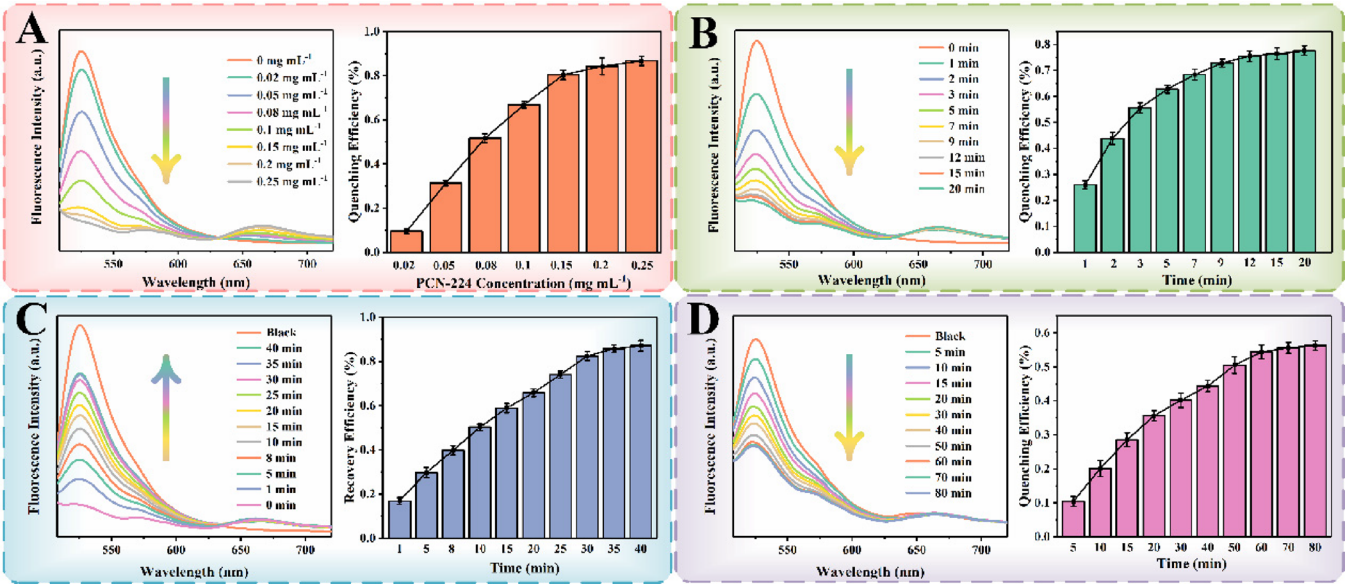

Figure 4. Fluorescence spectra and quenching efficiencies of FAM-ssDNA under (A) different concentrations of PCN-224 and (B) different times with 0.2 mg mL^{-1} PCN-224. (C) Fluorescence spectra and quenching efficiencies of FAM-ssDNA with 0.2 mg mL^{-1} PCN-224 under different times with 0.5 μM csDNA. (D) Fluorescence spectra and quenching efficiencies of FAM-ssDNA with 0.2 mg mL^{-1} PCN-224 and 0.5 μM csDNA under different times with 5 μM AA. All the experiments were conducted at 37 °C. λ_{ex} = 480 nm.

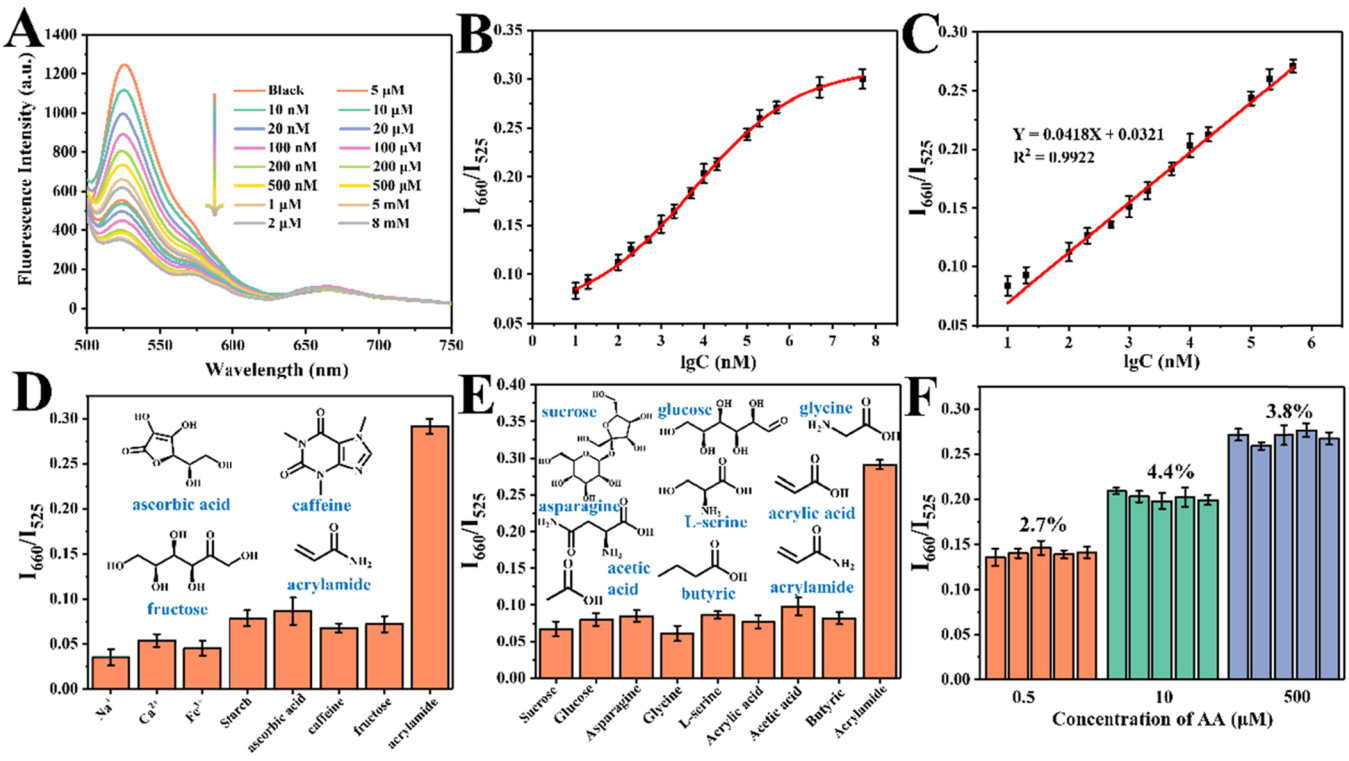

Figure 5. (A) Fluorescence spectra of FAM-ssDNA with 0.2 mg mL^{-1} PCN-224 and 0.5 μM csDNA for the detection of different concentrations of AA (λ_{ex} = 480 nm, 37 °C). (B) Corresponding relationship and (C) standard curve between the fluorescence intensity ratio I_{660}/I_{525} and AA concentrations. (D,E) Selectivity analysis of the PCN-224 biosensor to AA (λ_{ex} = 480 nm, 37 °C). (F) Repeatability experiments of the PCN-224 biosensor under different concentrations of AA (n = 5) (λ_{ex} = 480 nm, 37 °C).

Moreover, PCN-224 has been reported to have similar properties to semiconductors. Hence, it was assumed that the PET quenching mechanism existed between PCN-224 and FAM-ssDNA. The quenching efficiencies of PCN-224, $ZrOCl_2{\cdot}8H_2O$, and H_2TCPP to FAM-ssDNA were measured to gain further insight into the quenching mechanism. As illustrated in Figure S3, both $ZrOCl_2{\cdot}8H_2O$ and H_2TCPP could quench the fluorescence of FAM-ssDNA, and their average fluorescence quenching efficiencies were 80.4 and 52.3%, respectively. Moreover, the fluorescence quenching efficiencies were lower than that of PCN-224 (87.1%). This indicated that Zr−O clusters in PCN-224 presented an

https://doi.org/10.1021/acs.jafc.2c04756
J. Agric. Food Chem. 2022, 70, 10065−10074

Table 1. Analyses of AA in Thermally Processed Food Samples (Mean ± SD)[a]

samples (N = 3)	added ($\mu g \cdot kg^{-1}$)	found ($\mu g \cdot kg^{-1}$)	recovery (%)	RSD (%)	found by HPLC ($\mu g \cdot kg^{-1}$)	recovery (%)	RSD (%)
potato chip	0	332.4 ± 19.2		4.7	330.4 ± 15.5		2.1
	300	644.9 ± 21.5	103.8	2.6	628.7 ± 17.6	99.5	4.4
	600	938.9 ± 18.1	102.0	5.1	924.6 ± 20.9	98.2	3.7
biscuit	0	622.1 ± 19.8		3.8	621.9 ± 19.4		4.6
	300	910.3 ± 23.1	98.1	1.7	934.8 ± 16.2	102.1	3.4
	600	1235.8 ± 20.7	102.2	3.4	1214.3 ± 24.1	98.8	3.0

[a]In the recovery test, concentrations of sequence additions are 300 and 600 $\mu g \cdot kg^{-1}$.

important role in fluorescence quenching. A possible consequence of the insertion of Zr^{4+} into base pairs of FAM-ssDNA and the electrostatic binding to phosphate backbones provoked the PET process from FAM to Zr^{4+}. Under an excitation wavelength of 480 nm, the FAM dye changed to the excited state, and its photogenerated electrons were transferred to the Zr−O cluster with high electron-accepting capacity, which resulted in the fluorescence quenching of the FAM dye. To verify the PET quenching mechanism, we conducted electrochemical experiments to determine the higher occupied molecular orbital (HOMO) and the lower unoccupied molecular orbital (LUMO) of the FAM dye and Zr−O. The oxidation potential (E_{OX}) of FAM was −0.264 (Figure 3G). The reduction potential (E_{red}) and E_{OX} of Zr−O were 0.678 and 1.245 eV, respectively (Figure 3H). According to the previous reports,[34] the LUMO of FAM and Zr−O were 0.329 and −5.478 eV, respectively. The HOMO of FAM and Zr−O were −4.536 and −6.045 eV, respectively. Obviously, the LUMO of FAM was higher than that of Zr−O, which resulted in the transfer of electrons from FAM to Zr−O. As a result, when FAM-ssDNA was absorbed onto the surface of PCN-224, the FRET and PET between the FAM dye and PCN-224 contributed to the fluorescence quenching of the FAM dye.

Stepwise Optimizations of the Assay. The experimental conditions were optimized to improve the sensitivity of this method. First, the fluorescence quenching efficiency of three types of buffers was optimized. The results are shown in Figure S4, where the Tris−HCl buffer demonstrated a higher quenching effect (87.1%) compared to the HEPES buffer (84%) and PBS buffer (70.5%). Thus, Tris−HCl buffer was chosen as the buffer for further experiments. Then, the concentration of PCN-224 and the incubation time were optimized. The fluorescence intensity of FAM-ssDNA decreased significantly when the concentration of PCN-224 was increased (Figure 4A). The satisfactory quenching efficiency was obtained at 0.2 mg mL^{-1} of PCN-224. Meanwhile, the fluorescence intensity of FAM-ssDNA declined significantly within 12 min after the addition of 0.2 mg mL^{-1} PCN-224 (Figure 4B). Therefore, 12 min was set as the optimal incubation time for PCN-224 and FAM-ssDNA. To investigate the optimal incubation time of FAM-ssDNA with csDNA and AA, the fluorescence intensity of the compound FAM-ssDNA/PCN-224 in the existence of csDNA and AA/csDNA was monitored over time, respectively. FAM-ssDNA could hybridize with csDNA to form FAM-dsDNA, which could be released from the surface of PCN-224. The fluorescence intensity did not increase further after 35 min of incubation, indicating that FAM-ssDNA and csDNA had attained their maximum conjugation (Figure 4C). Compared with other MOF-based quenchers listed in Table S2, PCN-224 exhibited a faster and more effective recovery efficiency. The hybridization of FAM-ssDNA with csDNA was hindered when the target AA was added. The suitable time for incubation of ssDNA and AA was 60 min as seen in Figure 4D. A similar incubation time to the currently reported AA detection was observed (Table S3). Thus, optimal experimental conditions for assay were utilized for subsequent analyses.

Analysis of AA. The fluorescence response of the proposed ratiometric fluorescence biosensor to AA was measured under optimal conditions. As illustrated in Figure 5A, as the AA concentration increased, the fluorescence intensity at 525 nm decreased, while the emission peak of the H_2TCPP ligand at 660 nm remained unchanged, resulting in the ratiometric detection of AA. PCN-224 could absorb the single-stranded FAM-ssDNA to its surface and quench the fluorescence of FAM-ssDNA. The csDNA could hybridize with FAM-ssDNA to form FAM-dsDNA and be released from the surface of PCN-224. However, AA could destroy the hybridization process of csDNA and FAM-ssDNA. Thus, PCN-224 quenched the unhybridized FAM-ssDNA. Figure 5B presents evident and consistent tendencies of AA-deduced inhibition over a wide range of concentrations, from 10 nM to 0.5 mM. Particularly, a pleasurable log-liner relationship, between the AA concentration and fluorescence intensity ratio I_{660}/I_{525}, was established with the proposed biosensor (Figure 5C). Furthermore, the LOD was calculated to be 1.9 nM with 3 times noise in blank as the accepted standard. Such a low LOD could greatly satisfy the demands of AA detection in various food samples, such as the EU regulations of 300−850 $\mu g \cdot kg^{-1}$ for maximum residue levels. We extensively summarized primary features of this biosensor and other valuable studies in Table S4. The fabricated PCN-224 biosensor not only realized the ratiometric detection of AA but also broadened the detection range and improved the detection sensitivity as compared to a previously reported fluorescent sensor. Moreover, the fluorescent color of the ratiometric fluorescence biosensor can vary with the change of AA (from yellowish-green to yellow-green), which was not possible with a single fluorescent sensor (Figure S5). Significantly, this biosensor also showed distinct fluorescence responses within 60 d, which could play an important role in the rapid analysis of AA in foodstuffs (Figure S6).

Selectivity and Reproducibility of the Assay. The selectivity performances of the biosensor against interfering substances were investigated. A wide range of sucrose, glucose, asparagine, glycine, L-serine, acrylic acid, acetic acid, butyric acid, Na^+, Ga^{2+}, Fe^{3+}, starch, ascorbic acid, caffeine, and fructose were examined to study the selectivity of the proposed biosensor under optimal conditions. As depicted in Figure 5D,E, I_{660}/I_{525} for AA was obviously superior to those for other substances. These results indicated that the designed assay presented remarkable selectivity and specificity for AA detection, which was consistent with a study reported previously.[20] In this regard, the potential interference

https://doi.org/10.1021/acs.jafc.2c04756
J. Agric. Food Chem. 2022, 70, 10065−10074

substances were unable to interact with FAM-ssDNA, allowing csDNA to hybridize with FAM-ssDNA and form dsDNA, which in turn results in the release from the surface of PCN-224. Finally, the fluorescence of FAM-ssDNA was restored. The specific recognition between AA and the guanine base of its aptamers should account for such high selectivity. Considering the complexity of the real samples, the reproducibility of the assay for AA detection was assessed by five repetitive assays at three concentration levels. As demonstrated by Figure 5F, satisfied relative standard deviation (RSD) ranges of 2.7−4.4% for AA were obtained, indicating the excellent reproducibility of the proposed biosensor. The biosensor showed promising potential for high-performance AA sensing owing to these advantages.

Application in Real Samples. The proposed assay's effectiveness as a ratiometric fluorescence biosensor to detect AA was investigated using potato chips and biscuit samples. The results revealed acceptable recoveries in the ranges of 94.7 and 104.3% with RSDs ranging from 2.9 to 5.4% (Table 1). The acquired results revealed that the proposed biosensor exhibited favorable detection reliability. Moreover, these findings were also consistent with HPLC results (Figure S7). Thus, the biosensor fabricated in the study has a great deal of potential for food and environmental analyses.

The ratiometric biosensor was successfully fabricated for ultrasensitive and high selectivity detection of AA by using FAM-ssDNA and PCN-224 as the multifunctional sensing element. The PCN-224 biosensor has three functions: (1) PCN-224 works as a quencher for FAM-ssDNA; (2) the H_2TCPP ligand provides an intrinsic fluorescence; (3) FAM-ssDNA acts as a specific unit to recognize the analyte AA. The fluorescence of FAM-ssDNA was restored after hybridization. The highly sensitive detection of AA was achieved by impeding the hybridization of FAM-ssDNA with csDNA. The fabricated biosensor was successfully used in the analysis of potato chips and cookie samples. The detection results were consistent with those obtained by HPLC. The proposed biosensor exhibited excellent potential for practical application in food and environmental analysis owing to its superior characteristics.

■ ASSOCIATED CONTENT

Supporting Information

The Supporting Information is available free of charge at https://pubs.acs.org/doi/10.1021/acs.jafc.2c04756.

EDS mapping analysis of PCN-224 absorbed with FAM-ssDNA; high-resolution XPS response of the Zr 3d core energy levels of PCN-224; fluorescence quenching spectra of FAM-ssDNA (0.5 μM) in PCN-224, Zr−O, and H_2TCPP solution at a concentration of 0.2 mg mL^{-1} (excitation wavelength, 480 nm), fluorescence quenching efficiencies of FAM-ssDNA in PCN-224, Zr−O, and H_2TCPP solution; influence of different buffers at pH 7.4 (FAM-ssDNA, 0.5 μM; PCN-224, 0.2 mg mL^{-1}; incubation time, 12 min); CIE coordinate diagram of FAM-ssDNA with 0.2 mg mL^{-1} PCN-224 and 0.5 μM csDNA for the detection of different concentrations of AA (λ_{ex} = 480 nm, 37 °C); fluorescence stability of PCN-224 up to 60 days (RSD: 3.1%); HPLC spectra of AA and real samples (biscuit and potato chip) spiked with AA; fluorescence lifetimes of FAM-ssDNA and FAM-ssDNA mixed with PCN-224; comparison of the fluorescence quenching properties of MOFs; comparison of the incubation time of our biosensor with a previously reported method for AA detection; and comparison of our developed biosensor with a previously reported method for AA detection (PDF)

■ AUTHOR INFORMATION

Corresponding Authors

Jiyong Shi − *School of Food and Biological Engineering, Jiangsu University, Zhenjiang 212013, China; International Joint Research Laboratory of Intelligent Agriculture and Agri-products Processing (Jiangsu Education Department), Zhenjiang 212013, China;* orcid.org/0000-0002-4073-8304; Phone: +86 511 88780085; Email: Shi_jiyong@ujs.edu.cn; Fax: +86 511 88780201

Xiaobo Zou − *School of Food and Biological Engineering, Jiangsu University, Zhenjiang 212013, China; International Joint Research Laboratory of Intelligent Agriculture and Agri-products Processing (Jiangsu Education Department), Zhenjiang 212013, China;* orcid.org/0000-0001-5719-7025; Phone: +86 511 88780085; Email: zou_xiaobo@ujs.edu.cn; Fax: +86 511 88780201

Authors

Ziyu Gan − *School of Food and Biological Engineering, Jiangsu University, Zhenjiang 212013, China; International Joint Research Laboratory of Intelligent Agriculture and Agri-products Processing (Jiangsu Education Department), Zhenjiang 212013, China*

Wen Zhang − *School of Food and Biological Engineering, Jiangsu University, Zhenjiang 212013, China; International Joint Research Laboratory of Intelligent Agriculture and Agri-products Processing (Jiangsu Education Department), Zhenjiang 212013, China;* orcid.org/0000-0002-6851-0651

Muhammad Arslan − *School of Food and Biological Engineering, Jiangsu University, Zhenjiang 212013, China; International Joint Research Laboratory of Intelligent Agriculture and Agri-products Processing (Jiangsu Education Department), Zhenjiang 212013, China*

Xuetao Hu − *School of Food and Biological Engineering, Jiangsu University, Zhenjiang 212013, China; International Joint Research Laboratory of Intelligent Agriculture and Agri-products Processing (Jiangsu Education Department), Zhenjiang 212013, China*

Xinai Zhang − *School of Food and Biological Engineering, Jiangsu University, Zhenjiang 212013, China; International Joint Research Laboratory of Intelligent Agriculture and Agri-products Processing (Jiangsu Education Department), Zhenjiang 212013, China;* orcid.org/0000-0002-3901-0148

Zhihua Li − *School of Food and Biological Engineering, Jiangsu University, Zhenjiang 212013, China; International Joint Research Laboratory of Intelligent Agriculture and Agri-products Processing (Jiangsu Education Department), Zhenjiang 212013, China*

Complete contact information is available at: https://pubs.acs.org/10.1021/acs.jafc.2c04756

Author Contributions

The manuscript was written through contributions of all authors. All authors have given approval to the final version of the manuscript.

Notes

The authors declare no competing financial interest.

■ ACKNOWLEDGMENTS

The authors gratefully acknowledge the financial support provided by the Postdoctoral Science Foundation of China (2021M691319), the National Natural Science Foundation of China (31772073 and 32150410347), the Natural Science Foundation of Jiangsu Province (BE2019359), the Jiangsu Specially-Appointed Professor Project (20TPJS074), and Priority Academic Program Development of Jiangsu Higher Education Institutions (PAPD).

■ REFERENCES

(1) Li, N.; Liu, X.; Zhu, J.; Zhou, B.; Jing, J.; Wang, A.; Xu, R.; Wen, Z.; Shi, X.; Guo, S. Simple and Sensitive Detection of Acrylamide Based on Hemoglobin Immobilization in Carbon Ionic Liquid Paste Electrode. *Food Control* **2020**, *109*, No. 106764.

(2) WHO. *IARC Monographs on the Evaluation of Carcinogenic Risks to Humans*; List Iarc Eval., 1995.

(3) Mottram, D. S.; Wedzicha, B. L.; Dodson, A. T. Acrylamide Is Formed in the Maillard Reaction. *Nature* **2002**, *419*, 448−449.

(4) Rayappa, M. K.; Viswanathan, P. A.; Rattu, G.; Krishna, P. M. Nanomaterials Enabled and Bio/Chemical Analytical Sensors for Acrylamide Detection in Thermally Processed Foods: Advances and Outlook. *J. Agric. Food Chem.* **2021**, *69*, 4578−4603.

(5) Zhuang, Y.-T.; Ma, L.; Huang, H.; Han, L.; Wang, L.; Zhang, Y. A Portable Kit Based on Thiol-Ene Michael Addition for Acrylamide Detection in Thermally Processed Foods. *Food Chem.* **2022**, *373*, No. 131465.

(6) Zhang, C.; Shi, X.; Yu, F.; Quan, Y. Preparation of Dummy Molecularly Imprinted Polymers Based on Dextran-Modified Magnetic Nanoparticles Fe3O4 for the Selective Detection of Acrylamide in Potato Chips. *Food Chem.* **2020**, *317*, No. 126431.

(7) Cheng, J.; Zhang, S.; Wang, S.; Wang, P.; Su, X.-O.; Xie, J. Rapid and Sensitive Detection of Acrylamide in Fried Food Using Dispersive Solid-Phase Extraction Combined with Surface-Enhanced Raman Spectroscopy. *Food Chem.* **2019**, *276*, 157−163.

(8) Cheng, W.; Wang, X.; Zhang, Z.; Ma, L.; Liu, G.; Wang, Q.; Chen, F.; Cheng, K.-W. Development of an Isotope Dilution UHPLC−QqQ-MS/MS-Based Method for Simultaneous Determination of Typical Advanced Glycation End Products and Acrylamide in Baked and Fried Foods. *J. Agric. Food Chem.* **2021**, *69*, 2611−2618.

(9) Qin, L.; Zhang, Y.-Y.; Xu, X.-B.; Wang, X.-S.; Liu, H.-W.; Zhou, D.-Y.; Zhu, B.-W.; Thornton, M. Isotope Dilution HPLC-MS/MS for Simultaneous Quantification of Acrylamide and 5-Hydroxymethylfurfural (HMF) in Thermally Processed Seafood. *Food Chem.* **2017**, *232*, 633−638.

(10) Huang, S.-S.; Chen, D.; Wu, H.; Chen, R.-C.; Du, S.-J.; Dong, J.-J.; Liang, G.; Xu, L.-M.; Wang, X.-D.; Yang, Y.-P.; Yu, Z.-P.; Feng, W.-K.; Chen, Y.-P. Cannabinoid Receptors Are Involved in the Protective Effect of a Novel Curcumin Derivative C66 against CCl4-Induced Liver Fibrosis. *Eur. J. Pharmacol.* **2016**, *779*, 22−30.

(11) Zhao, D.; Zhang, Y.; Ji, S.; Lu, Y.; Bai, X.; Yin, M.; Huang, C.; Jia, N. Molecularly Imprinted Photoelectrochemical Sensing Based on ZnO/Polypyrrole Nanocomposites for Acrylamide Detection. *Biosens. Bioelectron.* **2021**, *173*, No. 112816.

(12) Luo, L.; Jia, B.-Z.; Wei, X.-Q.; Xiao, Z.-L.; Wang, H.; Sun, Y.-M.; Shen, Y.-D.; Lei, H.-T.; Xu, Z.-L. Development of an Inner Filter Effect-Based Fluorescence Immunoassay for the Detection of Acrylamide Using 9-Xanthydrol Derivatization. *Sens. Actuators, B* **2021**, *332*, No. 129561.

(13) Wei, Q.; Liu, T.; Pu, H.; Sun, D.-W. Determination of Acrylamide in Food Products Based on the Fluorescence Enhancement Induced by Distance Increase between Functionalized Carbon Quantum Dots. *Talanta* **2020**, *218*, No. 121152.

(14) Asnaashari, M.; Esmaeilzadeh Kenari, R.; Farahmandfar, R.; Taghdisi, S. M.; Abnous, K. Fluorescence Quenching Biosensor for Acrylamide Detection in Food Products Based on Double-Stranded DNA and Gold Nanoparticles. *Sens. Actuators, B* **2018**, *265*, 339−345.

(15) Gan, Z.; Zhang, W.; Shi, J.; Xu, X.; Hu, X.; Zhang, X.; Wang, X.; Arslan, M.; Xiao, J.; Zou, X. Collaborative Compounding of Metal-Organic Frameworks and Lanthanide Coordination Polymers for Ratiometric Visual Detection of Tetracycline. *Dyes Pigm.* **2021**, *194*, No. 109545.

(16) Gan, Z.; Hu, X.; Huang, X.; Li, Z.; Zou, X.; Shi, J.; Zhang, W.; Li, Y.; Xu, Y. A Dual-Emission Fluorescence Sensor for Ultrasensitive Sensing Mercury in Milk Based on Carbon Quantum Dots Modified with Europium (III) Complexes. *Sens. Actuators, B* **2021**, *328*, No. 128997.

(17) Du, P.; Niu, Q.; Chen, J.; Chen, Y.; Zhao, J.; Lu, X. "Switch-On" Fluorescence Detection of Glucose with High Specificity and Sensitivity Based on Silver Nanoparticles Supported on Porphyrin Metal−Organic Frameworks. *Anal. Chem.* **2020**, *92*, 7980−7986.

(18) Wang, J.; Fan, Y.; Tan, Y.; Zhao, X.; Zhang, Y.; Cheng, C.; Yang, M. Porphyrinic Metal−Organic Framework PCN-224 Nanoparticles for Near-Infrared-Induced Attenuation of Aggregation and Neurotoxicity of Alzheimer's Amyloid-β Peptide. *ACS Appl. Mater. Interfaces* **2018**, *10*, 36615−36621.

(19) Liu, S.; Bai, J.; Huo, Y.; Ning, B.; Peng, Y.; Li, S.; Han, D.; Kang, W.; Gao, Z. A Zirconium-Porphyrin MOF-Based Ratiometric Fluorescent Biosensor for Rapid and Ultrasensitive Detection of Chloramphenicol. *Biosens. Bioelectron.* **2020**, *149*, No. 111801.

(20) Wei, Q.; Zhang, P.; Liu, T.; Pu, H.; Sun, D.-W. A Fluorescence Biosensor Based on Single-Stranded DNA and Carbon Quantum Dots for Acrylamide Detection. *Food Chem.* **2021**, *356*, No. 129668.

(21) Park, J.; Jiang, Q.; Feng, D.; Mao, L.; Zhou, H.-C. Size-Controlled Synthesis of Porphyrinic Metal−Organic Framework and Functionalization for Targeted Photodynamic Therapy. *J. Am. Chem. Soc.* **2016**, *138*, 3518−3525.

(22) Asnaashari, M.; Kenari, R. E.; Farahmandfar, R.; Abnous, K.; Taghdisi, S. M. An Electrochemical Biosensor Based on Hemoglobin-Oligonucleotides-Modified Electrode for Detection of Acrylamide in Potato Fries. *Food Chem.* **2019**, *271*, 54−61.

(23) Luo, Y.; Liu, X.; Tan, L.; Li, Z.; Yeung, K. W. K.; Zheng, Y.; Cui, Z.; Liang, Y.; Zhu, S.; Li, C.; Wang, X.; Wu, S. Enhanced Photocatalytic and Photothermal Properties of Ecofriendly Metal-Organic Framework Heterojunction for Rapid Sterilization. *Chem. Eng. J.* **2021**, *405*, No. 126730.

(24) Min, T.; Sun, X.; Zhou, L.; Du, H.; Zhu, Z.; Wen, Y. Electrospun Pullulan/PVA Nanofibers Integrated with Thymol-Loaded Porphyrin Metal−organic Framework for Antibacterial Food Packaging. *Carbohydr. Polym.* **2021**, *270*, No. 118391.

(25) Nie, X.; Wu, S.; Liao, S.; Chen, J.; Huang, F.; Li, W.; Wang, Q.; Wei, Q. Light-Driven Self-Disinfecting Textiles Functionalized by PCN-224 and Ag Nanoparticles. *J. Hazard. Mater.* **2021**, *416*, No. 125786.

(26) Gan, Z.; Hu, X.; Xu, X.; Zhang, W.; Zou, X.; Shi, J.; Zheng, K.; Arslan, M. A Portable Test Strip Based on Fluorescent Europium-Based Metal−Organic Framework for Rapid and Visual Detection of Tetracycline in Food Samples. *Food Chem.* **2021**, *354*, No. 129501.

(27) Yuan, L.; Hou, W.; Xia, L.; Cheng, C.; Wan, S.; Jiang, Y.; Yang, Y.; Wu, Q.; Qiu, L.; Tan, W. ZrMOF Nanoparticles as Quenchers to Conjugate DNA Aptamers for Target-Induced Bioimaging and Photodynamic Therapy. *Chem. Sci.* **2018**, *9*, 7505−7509.

(28) Zhao, M.; Wang, Y.; Ma, Q.; Huang, Y.; Zhang, X.; Ping, J.; Zhang, Z.; Lu, Q.; Yu, Y.; Xu, H. Ultrathin 2D Metal−Organic Framework Nanosheets. *Adv. Mater.* **2016**, *27*, 7372−7378.

(29) Hao, Y.-B.; Shao, Z.-S.; Cheng, C.; Xie, X.-Y.; Zhang, J.; Song, W.-J.; Wang, H.-S. Regulating Fluorescent Aptamer-Sensing Behavior

of Zeolitic Imidazolate Framework (ZIF-8) Platform via Lanthanide Ion Doping. *ACS Appl. Mater. Interfaces* **2019**, *11*, 31755−31762.
(30) Zhu, X.; Li, B.; Yang, J.; Li, Y.; Zhao, W.; Shi, J.; Gu, J. Effective Adsorption and Enhanced Removal of Organophosphorus Pesticides from Aqueous Solution by Zr-Based MOFs of UiO-67. *ACS Appl. Mater. Interfaces* **2015**, *7*, 223−231.
(31) Tian, J.; Liu, Q.; Shi, J.; Hu, J.; Asiri, A. M.; Sun, X.; He, Y. Rapid, Sensitive, and Selective Fluorescent DNA Detection Using Iron-Based Metal−Organic Framework Nanorods: Synergies of the Metal Center and Organic Linker. *Biosens. Bioelectron.* **2015**, *71*, 1−6.
(32) Qiu, Y.; Qu, X.; Dong, J.; Ai, S.; Han, R. Electrochemical Detection of DNA Damage Induced by Acrylamide and Its Metabolite at the Graphene-Ionic Liquid-Nafion Modified Pyrolytic Graphite Electrode. *J. Hazard. Mater.* **2011**, *190*, 480−485.
(33) Lu, C.-H.; Guo, W.; Hu, Y.; Qi, X.-J.; Willner, I. Multitriggered Shape-Memory Acrylamide−DNA Hydrogels. *J. Am. Chem. Soc.* **2015**, *137*, 15723−15731.
(34) Wu, Z.; Ji, C.; Zhao, X.; Han, Y.; Müllen, K.; Pan, K.; Yin, M. Green-Light-Triggered Phase Transition of Azobenzene Derivatives toward Reversible Adhesives. *J. Am. Chem. Soc.* **2019**, *141*, 7385−7390.

https://doi.org/10.1021/acs.jafc.2c04756
J. Agric. Food Chem. 2022, 70, 10065−10074